COBEM2015

ABCM Associação Brasileira de Engenharia e Ciências Mecânicas

23rd ABCM International Congress of Mechanical Engineering
December 6-11, 2015, Rio de Janeiro, RJ, Brazil

NANO-PATTERNING OF SURFACES BY ION SPUTTERING: NUMERICAL STUDY OF THE DAMPING EFFECT ON THE ANISOTROPIC KURAMOTO-SIVASHINSKY EQUATION

Eduardo Vitral
José Pontes
Gusavo Rabello dos Anjos
Norberto Mangiavacchi
GESAR, UERJ, Rio de Janeiro, Brazil
eduardo.vitral@gmail.com
jose.pontes@uerj.br
gustavo.anjos@uerj.br
norberto@uerj.br

Daniel Walgraef
IFISC, University of Balearic Islands, Palma de Mallorca, Spain
dwalgraef@ifisc.uib-csic.es

Abstract. *This paper presents a numerical approach to a model describing the pattern formation by ion beam sputtering on a material surface. This process is responsible for the appearance of unexpectedly organized patterns, such as ripples, nanodots and hexagonal arrays of nanoholes. A numerical analysis of preexisting patterns is proposed to investigate surface dynamics, based on a model derived from a anisotropic damped Kuramoto-Sivashinsky equation, in a two dimensional surface with periodic boundary conditions. While deterministic, its highly nonlinear character gives a rich range of results, making it possible to describe accurately different patterns. A finite-difference semi-implicit splitting scheme is employed on the discretization of the governing equation. Simulations were conducted with realistic coefficients related to physical parameters (anisotropies, beam orientation, diffusion). The stability of the numerical scheme is verified with time step and grid spacing tests for the pattern evolution. Hexagonal patterns were obtained from a monomodal initial condition for a higher value of the damping coefficient α, while spatiotemporal chaos appeared for lower values. The hexagonal ordered character of the structure was shown to be directly proportional to α.*

Keywords: *Kuramoto-Sivashinsky equation, sputtering, finite-difference method, pattern formation*

1. INTRODUCTION

Sputtering is a phenomenon which leads to the ejection of atoms from a solid surface, as a result of an ion beam incidence or glow discharge. It is a technique which operates in nonequilibrium conditions, permitting the processing of nano-structures beyond the limitations imposed by equilibrium thermodynamics. The present endeavor is interested in the spontaneous well-ordered periodicity developed by ion beam sputtering, which appears over a large area under certain conditions (Chason and Chan, 2010). Modeling the nonlinear evolution of sputter-eroded surfaces is an ongoing mathematical challenge. Our effort aims toward the development of a numerical scheme to solve an anisotropic Kuramoto-Sivashisnky equation with realistic coefficients, since it produces a rich zoology that can be adjusted to represent the aforementioned erosion dynamics.

If the energy of the incident ion is sufficient, a train of collision event may be established, resulting in the removal of atoms from the solid surface. The morphology of the surface can drastically change due to these sputtered atoms, and it may result in the formation of unexpectedly organized patterns, such as ripples, nanodots and hexagonal arrays of nanoholes (see Ghoniem *et al.* (2015), Mollick *et al.* (2014) and Wei *et al.* (2009)). Valbusa *et al.* (2002) discussed the interplay between ion erosion and vacancies on the surface re-organization, which would explain some of the patterns experimentally detected. The rate of energy deposition is a crucial parameter for the mechanisms, since high values can lead to a local transient melting of the surface (Mollick *et al.*, 2014), alongside the possibility of ion implantation.

The Kuramoto-Sivashinsky equation appears from the continuum theories, in their attempt to describe surfaces eroded by ion bombardment, which would ultimately reproduce ripple formation and other organized patterns behavior. This equation was initially formulated to describe flame fronts and chemical waves (Makeev *et al.*, 2002), being capable of producing a great variety of morphologies for its highly nonlinear and deterministic character. Rost and Krug (1995) describe the equation as being remarkable for the stabilization of the linear instability by the nonlinear term. This sta-

bilization makes the equation a good candidate to represent the complexity behind the structure formation on sputtered surfaces, with a dynamic transiting between different regimes.

We propose a finite-difference semi-implicit splitting scheme of second order in time and space to numerically solve an anisotropic damped Kuramoto-Sivashinsky (DKS) equation subjected to periodical boundary conditions. The domain is a two dimensional surface defined by a height function $h(x, y, t)$, whose evolution in time is monitored. Internal iterations are used inside each time step to enhance the approximation of the nonlinear term. Previously, a similar numerical scheme was successfully implemented for the Swift-Hohenberg Equation by (Christov *et al.*, 1997) and citepchristov2002numerical, which also dealt with the challenges of high-order spatial derivatives and nonlinearity.

The stability of the numerical scheme is verified with time step and grid spacing tests for the pattern evolution, and the simulation results are discussed based on the sputtering physics, previous studies regarding the damping effect on the DKS equation and linear stability analysis predictions. Hexagonal patterns were obtained from a monomodal initial condition in the $\vec{1}_x$ direction for a higher value of the damping coefficient α, while spatiotemporal chaos appeared for lower values. The hexagonal character of the structure was shown to be directly proportional to α, even for spatiotemporal chaos results.

2. MATERIAL AND METHODS

2.1 Governing Equations

The present study proposes a second order in time finite difference numerical scheme for solving modifications of the generalized Kuramoto-Sivashinsky equation (Sigmund, 1969; Bradley and Harper, 1988; Cuerno and Barabási, 1995; Valbusa *et al.*, 2002; Makeev *et al.*, 2002). For the case of isotropic energy distribution, considering an ion beam with angle of incidence θ with respect to the normal of the surface, one dimensionless and simplified form of the equation reads:

$$\begin{aligned}\frac{\partial \bar{h}}{\partial \tau} &= -\bar{\alpha}\bar{h} + \bar{\mu}\frac{\partial^2 \bar{h}}{\partial X^2} - c^2\frac{\partial^2 \bar{h}}{\partial Y^2} + \bar{\nu}_x\left(\frac{\partial \bar{h}}{\partial X}\right)^2 - c^3\left(\frac{\partial \bar{h}}{\partial Y}\right)^2 \\ &\quad -D_{XX}\frac{\partial^4 \bar{h}}{\partial X^4} + D_{XY}\frac{\partial^4 \bar{h}}{\partial X^2 \partial Y^2} + c^2\frac{\partial^4 \bar{h}}{\partial Y^4} - \bar{K}\left(\frac{\partial^4 \bar{h}}{\partial X^4} + 2\frac{\partial^4 \bar{h}}{\partial X^2 Y^2} + \frac{\partial^4 \bar{h}}{\partial Y^4}\right) \end{aligned} \quad (1)$$

where $\bar{h}$ and τ are, respectively, the surface height function of the external atom layer and the time dependency of the transient model, with X and Y as the domain space coordinates. The function c represents the cosine of the incident angle θ. Equation 1 presents a damping term $-\alpha\bar{h}$, with α being a damping coefficient, contributing to the smoothening of the surface (Keller and Facsko, 2010). Finally, K takes into account the surface diffusion effects, which varies with temperature. The parameters μ, μ_x, D_{xx} and D_{xy} will be defined as follows:

$$\begin{aligned}\bar{\mu} &= 2s^2 - c^2 - a_\mu^2 s^2 c^2 \\ \bar{\nu}_x &= c\left(3s^2 - c^2 - a_\mu^2 s^2 c^2\right) \\ D_{XX} &= \left(c^2 - 4s^2 + 2a_\mu^2 s^2\left(c^2 - \frac{2}{3}s^2\right) + \frac{a_\mu^4}{3}s^4 c^2\right) \\ D_{XY} &= 2\left(c^2 - 2s^2 + a_\mu^2 s^2 c^2\right)\end{aligned}$$

Here, s is the sine of θ and a_μ is the ratio between the ionic penetration depth and the width of energy distribution. In order to solve Equation 1, the following second order in time Cranck-Nicholson semi-implicit scheme was adopted:

$$\frac{\bar{h}^{n+1} - \bar{h}^n}{\Delta\tau} = \Lambda_X\left(\bar{h}^{n+1} + \bar{h}^n\right) + \Lambda_Y\left(\bar{h}^{n+1} + \bar{h}^n\right) + f^{n+1/2}. \quad (2)$$

The superscript $(n+1)$ refers to the current time and (n) to the previous one. The operators $\Lambda_X^{n+1/2}$, $\Lambda_Y^{n+1/2}$ and the function $f^{n+1/2}$ are defined as:

$$\Lambda_X = \frac{1}{2}\left[-\frac{\bar{\alpha}}{2} - (D_{XX}+K)\frac{\partial^4}{\partial X^4}\right]$$

$$\Lambda_Y = \frac{1}{2}\left[-\frac{\bar{\alpha}}{2} - K\frac{\partial^4}{\partial Y^4}\right]$$

$$f^{n+1/2} = \frac{1}{2}\left[\bar{\mu}\frac{\partial^2}{\partial X^2} - c^2\frac{\partial^2}{\partial Y^2} + \bar{\nu}_X\left(\frac{\partial \bar{h}^{n+1}}{\partial X} + \frac{\partial \bar{h}^n}{\partial X}\right)\frac{\partial}{\partial X} - c^2\left(\frac{\partial \bar{h}^{n+1}}{\partial Y} + \frac{\partial \bar{h}^n}{\partial Y}\right)\frac{\partial}{\partial Y} + (D_{XY}-2K)\frac{\partial^4}{\partial X^2 \partial Y^2} + c^2\frac{\partial^4}{\partial Y^4}\right]\left(\bar{h}^{n+1}+\bar{h}^n\right)$$

2.2 Internal Iterations

Internal iterations at each time step are required to secure the approximation for the nonlinearities taking part in the scheme of Equation 2. The iterations loop will continue until convergence is attained from monitoring the L_∞ norm. There is a trade-off related to the time step $\Delta\tau$: for a larger $\Delta\tau$, convergence will be impaired and the number of internal iterations will increase, while a smaller $\Delta\tau$ will impact on a smaller number of iterations, but it will imply on a greater number of time steps. The internal iterations scheme reads:

$$\frac{\bar{h}^{n,m+1} - \bar{h}^n}{\Delta\tau} = \Lambda_X\left(\bar{h}^{n,m+1}+\bar{h}^n\right) + \Lambda_Y\left(\bar{h}^{n,m+1}+\bar{h}^n\right) + f^{n+1/2} \tag{3}$$

where the index m refers to the internal iteration number. The superscript $(n, m+1)$ identifies the new iteration, while (n) are the values of the previous time step. The superscript $(n+1)$ for the nonlinear term in the function $f^{n+1/2}$ will be replaced by (n, m), which stands for the values obtained from the previous iteration. The iterations proceed until the following criterion for the L_∞ norm is satisfied:

$$L_\infty = \frac{max\ |\bar{h}^{n,m+1} - \bar{h}^{n,m}|}{max\ |\bar{h}^{n,m+1}|} < 10^{-7} \tag{4}$$

for all points of the grid for a fixed m. The function $\bar{h}^{n+1}$ for the current time will be acquired from $\bar{h}^{n,m+1}$, proceeding to the last iteration.

2.3 The Splitting Scheme

The splitting of Equation 2 is made according to the second Douglas scheme (Douglas and Rachford, 1956; Yanenko, 1971). Such strategy has been chosen to deal with the costly procedure of solving Equation 2; even though we are working with sparse matrices for the operators, the internal iterations cause the process to be repeated several times during each time step. This problem welcomes an attempt to minimize the operations per unit iteration, as follows:

$$\frac{\tilde{\bar{h}} - \bar{h}^n}{\Delta\tau} = \Lambda_X\,\tilde{\bar{h}} + \Lambda_Y\,\bar{h}^n + f^{n+1/2} + (\Lambda_X+\Lambda_Y)\,\bar{h}^n \tag{5}$$

$$\frac{\bar{h}^{n,m+1} - \tilde{\bar{h}}}{\Delta\tau} = \Lambda_Y\left(\bar{h}^{n,m+1} - \bar{h}^n\right) \tag{6}$$

Here, $\tilde{\bar{h}}$ is the height function for the *half-time* step. Not only can it be shown that the splitting represents the original scheme, but it is also more stable than the original.

2.4 Scheme Stability

One important issue which concerns the simulations is the time and mesh size selection, since we must maintain the semi-implicit scheme stable. Here, we study the time step and grid spacing variation effect regarding the pattern evolution, which is translated by the L_1 norm curve. The computational effort was also measured, being related to the number of internal iterations when comparing results for a same grid spacing.

1. Case 1: ΔX = 2, 64×64 points in a domain 128×128

2. Case 2: ΔX = 1, 128×128 points in a domain 128×128

Both cases start with a monomodal initial pattern $q_o\vec{1}_x$, presenting four wavelengths in the domain. The critical wavelength (related to critical wavenumber q_c) is approximately 18: each of them would be represented by 9 points for Case 1 and by 18 points for Case 2. The parameters adopted for the tests are displayed in Table 1.

Table 1: Parameters value and description

Parameter	Value	Description
$\bar{\alpha}$	0.15	damping coefficient
$\bar{K}$	5	surface diffusion effects
θ	30°	beam's angle of incidence
a_μ	4	penetration depth/width of energy distribution

During the simulations, we monitored the pattern's rate of evolution by the L_1 norm, which indicates how fast the structure is changing between the current and previous time step, normalized by the spatial average of the modulus of the surface height. This norm is denoted as:

$$L_1 = \frac{\sum_{ij} |\bar{h}_{ij}^{n+1} - \bar{h}_{ij}^{n}|}{\Delta\tau \sum_{ij} |\bar{h}^{n+1}|} \tag{7}$$

We assumed a pattern as stationary if the criteria $L_1 < 10^{-7}$ was reached for the temporal evolution. On the other hand, the simulation would be stopped if the L_1 curve demonstrated clearly a behavior converging to a fixed value (or oscillating around it).

Figure 1 compares the structure evolution through the L_1 norm to observe when the results would diverge for an increasing time step.

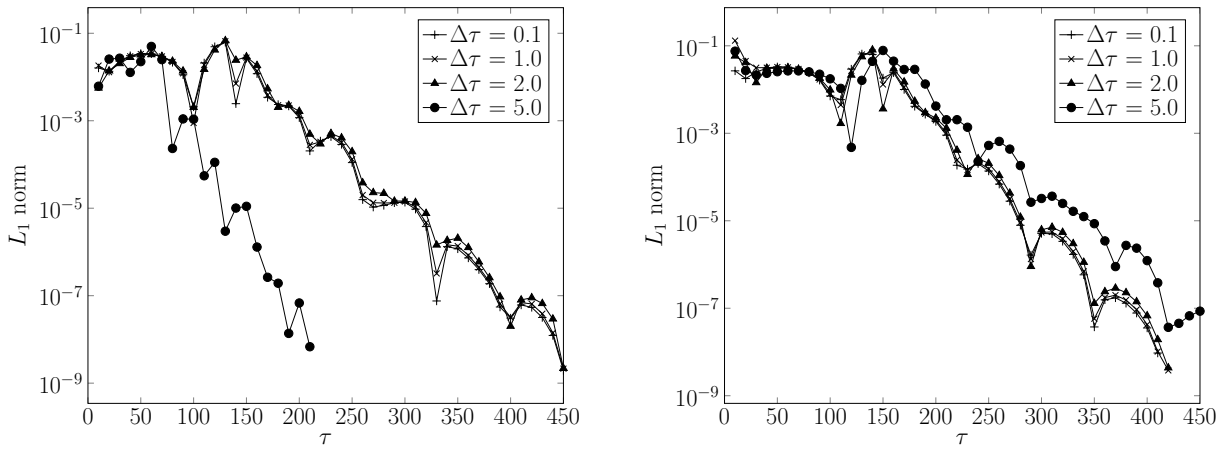

(a) Case 1: $\Delta X = 2$, 64×64 points in a domain 128×128

(b) Case 2: $\Delta X = 1$, 128×128 points in a domain 128×128

Figure 1: L_1 norm as a measure for stability regarding time step

From Figure 1a (Case 1) we observe slight deviations in the L_1 norm evolution for $\Delta\tau = 2.0$ when comparing to inferior time steps values, while $\Delta\tau = 5.0$ diverges completely from the others. Regarding Figure 1b (Case 2), the divergence for $\Delta\tau = 5.0$ is also clear, but it's more coherent with the smaller time steps than Case 1, as expected from a more refined mesh. This time, $\Delta\tau = 2.0$ is more consistent with the smaller ones, and would be accepted for the simulations. Even so, we decided to operate with $\Delta\tau = 1.0$ for $\Delta X = 1$, which is a more conservative approach.

3. RESULTS AND DISCUSSION

This study adopted the aforementioned time splitting finite-difference method to compare results for the two-dimensional DKS equation under 3 circumstances: $\alpha = 0$, $\alpha = 0.05$ and $\alpha = 0.15$. The mesh consisted of 512 × 512 points with a harmonic monomodal initial pattern in the $\vec{1}_x$ direction ($\vec{q} = q_o\vec{1}_x$), a small amplitude of 0.1, and parameters θ, K and a_μ

as found in Table 1. Since the side of the domain is $L_x = L_y = 512$, and the linear stability analysis reveals a value of $\lambda_c = 18$ for the critical wavelength corresponding to the maximum growth rate in the $\vec{1}_x$ direction, each wavelength of the final pattern was expected to be represented by 18 points.

According to the previous work of Paniconi and Elder (1997), three distinct solutions in the late time limit might be expected for the DKS equation, depending on the parameter α: periodic large hexagonal morphology for higher values, an oscillatory or breathing hexagonal state for middle values, and a spatiotemporal chaotic state for lower values. However, since the present endeavor considers realistic coefficients related to the physics of sputtering, the same range of α values employed by Paniconi and Elder (1997) wouldn't produce the same effects.

The undamped solution is shown in Figure 2, when $\alpha = 0$. The initial condition presented a wavenumber $q_o = 1.7181 \cdot 10^{-1}$ (14 wavelengths in the system). A disordered chaotic cellular structure is obtained for late time, with large variations of cell size and shape, as displayed in Figure 2a for $\tau = 11803$. From the L_1 curve (Figure 2b), we can see that the chaotic pattern is reached within $\tau = 500$. While a steady state isn't reached for the analyzed period, it's clear that the evolution dynamics are much slower during late time.

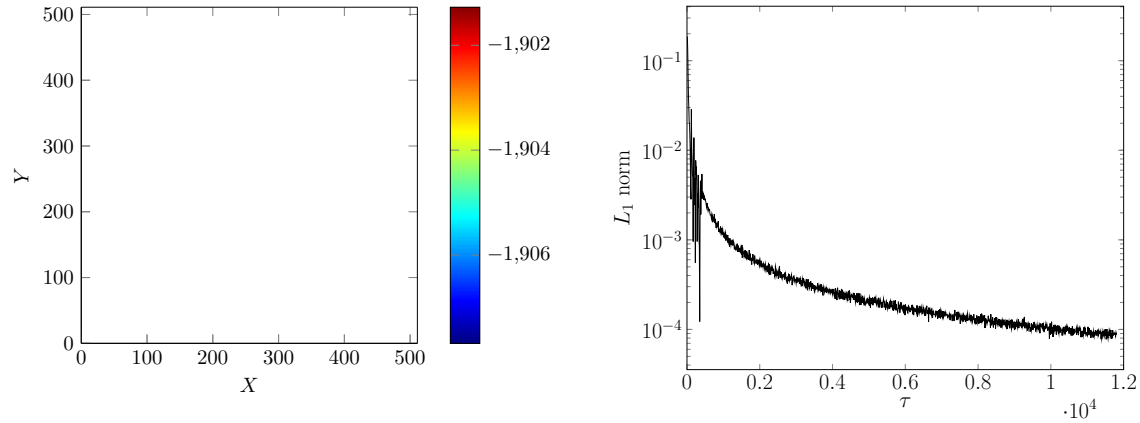

(a) Surface height $\bar{h}^n$ for $\tau = 11803$ (b) L_1 norm evolution

Figure 2: Numerical solution for a 2D anisotropic DKS equation - Spatiotemporal chaotic pattern, $\alpha = 0$

Figure 3 reveals the numerical solution for $\alpha = 0.05$. The initial condition was the same from the previous case ($q_o = 1.7181 \cdot 10^{-1}$) . A spatiotemporal chaotic cellular structure is obtained for late time, which can be seen in Figure 2a for $\tau = 11750$. In comparison with the undamped structure, the late time pattern for $\alpha = 0.05$ is much more organized, with a smaller variation of cells sizes and shape, and some of them approaching the λ_c width. The L_1 norm evolution (Figure 3b) shows that a strongly oscillatory state is reached by $\tau = 2000$, where L_1 starts fluctuating around $L_1 = 0.02$. These intense dynamics differ from the undamped case: even though the structure is more organized, it keeps changing at a constant rate for an undefined period of time.

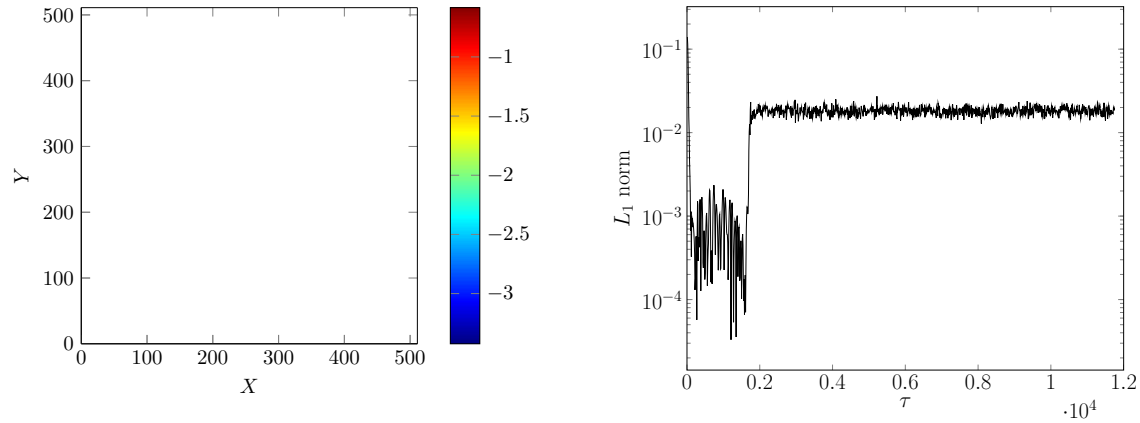

(a) Surface height $\bar{h}^n$ for $\tau = 11750$ (b) L_1 norm evolution

Figure 3: Numerical solution for a 2D anisotropic DKS equation - Chaotic semi-organized oscillatory behavior, $\alpha = 0.05$

For higher values of α, e.g. $\alpha = 0.15$, a defect-free hexagonal structure can be obtained, as displayed by Figure 4. A

smaller wavenumber $q_o = 2.4544 \cdot 10^{-2}$ was employed for the initial condition, since our previous studies revealed that an 1D structure with wavelength similar to λ_c would prevail for $q_o = 1.7181 \cdot 10^{-1}$ even in late time. Figure 4b shows that the L_1 norm has a first continuous decline, which represents the stabilization of an 1D structure with $\vec{q} \sim \vec{q_c}$. Even though this pattern seems to be approaching a steady state, hexagonal modes emerge when τ is approaching $\tau = 2000$, leading to a fast growth of L_1 and to the formation of a new structure. Posteriorly, L_1 reaches a peak and the structure initiates its final stabilization, quickly removing defects and falling until the stationary state, which is illustrated by Figure 4a for $\tau = 14630$.

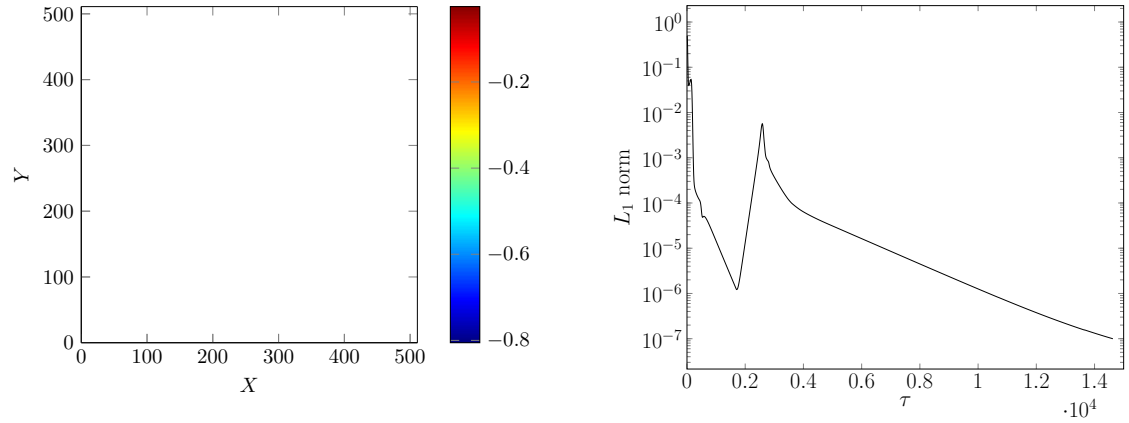

(a) Surface height $\bar{h}^n$ for $\tau = 14630$

(b) L_1 norm evolution

Figure 4: Numerical solution for a 2D anisotropic DKS equation - Stationary hexagonal structure, $\alpha = 0.15$

Comparing the structure evolution for $\alpha = 0.15$ and $\alpha = 0.05$, we confirm the coincident time for the emergence of the hexagonal modes, close to $\tau = 2000$. For $\alpha = 0.15$, the damping effect is sufficient for an ordered and quick reorganization of the structure after a L_1 peak, while for $\alpha = 0.05$ the damping is not high enough to allow the microstructure to reorganize itself into a perfectly ordered hexagonal state, and it keeps chaotically oscillating around the peak L_1 value. Another observation is made towards the obtained height values. All of them are negative, being consistent with the erosive phenomenon. However, for $\alpha = 0$ the mean height of the surface falls continuously with time, while maintaining the distance $\bar{h}_{dif}$ between the minimum and maximum points around $\bar{h}_{dif} = 6.4$. For $\alpha = 0.05$ the mean height remains approximately constant, around -0.5 and -3.5 ($\bar{h}_{dif} \sim 3.0$), for an undefined time. Finally, for the steady state obtained with a damping $\alpha = 0.15$, the maximum and minimum height values were, respectively, -0.03 and -0.81 ($\bar{h}_{dif} = 0.78$).

4. CONCLUSION

In the present paper we have developed a finite-difference time splitting scheme to solve an anisotropic Kuramoto-Sivashinsky equation, which can describe a surface eroded by ion bombardment. Regarding its stability, the tests revealed that for $\Delta\tau \leq 2.0$, the numerical scheme was sufficiently stable with a grid spacing $\Delta X = 1.0$. Spatiotemporal chaotic structures appeared for the undamped case, whose dynamics fell continuously for the long time. A chaotic oscillatory pattern rose from the simulation with $\alpha = 0.05$, reaching a better ordered structure than the one for the undamped result, while maintaining a highly constant kinematic after the emergence of the hexagonal modes. Defectless hexagonal periodic structures were obtained for higher values of the damping coefficient, starting from a monomodal initial condition with $\vec{q} = q_o \vec{1}_x$. These results were physically consistent with the sputtering phenomenon, reproducing ripple and hexagonal pattern formation experimentally obtained by other authors. Future work will investigate a wider range of values for α.

5. ACKNOWLEDGEMENTS

Eduardo Vitral acknowledges a fellowship from the Coordination for the Improvement of Higher Education-CAPES (Brazil). A FAPERJ Senior Researcher Fellowship is acknowledged by José Pontes. Gustavo Anjos is granted by Science Without Borders/Young Talent Attraction program (CAPES).

6. REFERENCES

Bradley, R.M. and Harper, J.M., 1988. "Theory of ripple topography induced by ion bombardment". *Journal of Vacuum Science & Technology A*, Vol. 6, No. 4, pp. 2390–2395.

Chason, E. and Chan, W.L., 2010. "Spontaneous patterning of surfaces by low-energy ion beams". In *Materials Science with Ion Beams*, Springer, pp. 53–71.

Christov, C. and Pontes, J., 2002. "Numerical scheme for swift-hohenberg equation with strict implementation of lyapunov functional". *Mathematical and computer modelling*, Vol. 35, No. 1, pp. 87–99.

Christov, C., Pontes, J., Walgraef, D. and Velarde, M.G., 1997. "Implicit time splitting for fourth-order parabolic equations". *Computer methods in applied mechanics and engineering*, Vol. 148, No. 3, pp. 209–224.

Cuerno, R. and Barabási, A.L., 1995. "Dynamic scaling of ion-sputtered surfaces". *Physical review letters*, Vol. 74, No. 23, p. 4746.

Douglas, J. and Rachford, H.H., 1956. "On the numerical solution of heat conduction problems in two and three space variables". *Transactions of the American mathematical Society*, pp. 421–439.

Ghoniem, N., Sehirlioglu, A., Neff, A.L., Allain, J.P., Williams, B. and Sharghi-Moshtaghin, R., 2015. "Sputtering of molybdenum and tungsten nano rods & nodules irradiated with 150 ev argon ions". *Applied Surface Science*.

Keller, A. and Facsko, S., 2010. "Ion-induced nanoscale ripple patterns on si surfaces: theory and experiment". *Materials*, Vol. 3, No. 10, pp. 4811–4841.

Makeev, M.A., Cuerno, R. and Barabasi, A.L., 2002. "Morphology of ion-sputtered surfaces". *Nuclear Instruments and Methods in Physics Research Section B: Beam Interactions with Materials and Atoms*, Vol. 197, No. 3, pp. 185–227.

Mollick, S.A., Ghose, D. and Satpati, B., 2014. "Formation of au–ge nanodots by au- ion sputtering of ge". *Vacuum*, Vol. 99, pp. 289–293.

Paniconi, M. and Elder, K., 1997. "Stationary, dynamical, and chaotic states of the two-dimensional damped kuramoto-sivashinsky equation". *Physical Review E*, Vol. 56, No. 3, p. 2713.

Rost, M. and Krug, J., 1995. "Anisotropic kuramoto-sivashinsky equation for surface growth and erosion". *Physical review letters*, Vol. 75, No. 21, p. 3894.

Sigmund, P., 1969. "Theory of sputtering. i. sputtering yield of amorphous and polycrystalline targets". *Physical review*, Vol. 184, No. 2, p. 383.

Valbusa, U., Boragno, C. and de Mongeot, F.B., 2002. "Nanostructuring surfaces by ion sputtering". *Journal of Physics: Condensed Matter*, Vol. 14, No. 35, p. 8153.

Wei, Q., Zhou, X., Joshi, B., Chen, Y., Li, K.D., Wei, Q., Sun, K. and Wang, L., 2009. "Self-assembly of ordered semiconductor nanoholes by ion beam sputtering". *Advanced Materials*, Vol. 21, No. 28, pp. 2865–2869.

Yanenko, N.N., 1971. *The method of fractional steps*. Springer.

7. RESPONSIBILITY NOTICE

The authors are the only responsible for the printed material included in this paper.